Broadening of Cloud Droplet Spectra through Eddy Hopping: Turbulent Adiabatic Parcel Simulations

WOJCIECH W. GRABOWSKI

National Center for Atmospheric Research,[a] *Boulder, Colorado, and Institute of Geophysics, Faculty of Physics, University of Warsaw, Warsaw, Poland*

GUSTAVO C. ABADE

Institute of Geophysics, Faculty of Physics, University of Warsaw, Warsaw, Poland

(Manuscript received 10 February 2017, in final form 16 March 2017)

ABSTRACT

This paper investigates spectral broadening of droplet size distributions through a mechanism referred to as the eddy hopping. The key idea, suggested a quarter century ago, is that droplets arriving at a given location within a turbulent cloud follow different trajectories and thus experience different growth histories and that this leads to a significant spectral broadening. In this study, the adiabatic parcel model with superdroplets is used to contrast droplet growth with and without turbulence. Turbulence inside the parcel is described by two parameters: (i) the dissipation rate of the turbulent kinetic energy ε and (ii) the linear extent of the parcel L. As expected, an adiabatic parcel without turbulence produces extremely narrow droplet spectra. In the turbulent parcel, a stochastic scheme is used to account for vertical velocity fluctuations that lead to local supersaturation fluctuations for each superdroplet. These fluctuations mimic the impact of droplets hopping turbulent eddies in a natural cloud. For L smaller than a few meters, noticeable spectral broadening is possible only for strong turbulence—say, $\varepsilon > 100\ \mathrm{cm^2\ s^{-3}}$. For L typical for grid lengths of large-eddy simulation (LES) models (say, L between 10 and 100 m), the impact is significant even with relatively modest turbulence intensities. The impact increases with both L and ε. The representation of eddy hopping developed in this paper can be included in a straightforward way in the subgrid-scale scheme of a Lagrangian LES cloud model and may lead to a significant acceleration of simulated rain development through collision–coalescence.

1. Introduction

Cloud droplets grow by the diffusion of water vapor before collisional growth turns them into drizzle and rain. A simple model of droplet growth inside an adiabatic parcel rising through a cumulus cloud gives extremely narrow droplet size distributions [e.g., Brenguier and Chaumat (2001) and references therein]. At the same time, observed distributions are typically wide and multimodal. This has already been observed in early cumulus studies nearly half a century ago (Warner 1969a,b, 1970, 1973a,b) and in many subsequent studies, including the recent ones in monsoon cumuli over India (Prabha et al. 2012). See the discussion and a comprehensive list of references in the introduction of Lasher-Trapp et al. (2005). Pawlowska et al. (2006) discuss observations of spectral width in marine stratocumulus. Cloud turbulence and turbulent entrainment are often invoked to explain this discrepancy [e.g., Jensen et al. (1985); Su et al. (1998); Lasher-Trapp et al. (2005); see also references in Grabowski and Wang (2013)]. However, quantitative studies targeting effects of turbulence on droplet size spectra are difficult because of the range of spatial and temporal scale involved, from hundreds of meters for energy-containing eddies down to the Kolmogorov microscale (around a millimeter in atmospheric turbulence) and because of the multiphase cloud environment.

The study reported in this paper investigates the mechanism affecting diffusional growth of droplets in turbulent clouds referred to as the eddy hopping, the term introduced in Grabowski and Wang (2013). The

[a] The National Center for Atmospheric Research is sponsored by the National Science Foundation.

Corresponding author e-mail: Wojciech W. Grabowski, grabow@ucar.edu

DOI: 10.1175/JAS-D-17-0043.1

key idea is that droplets arriving at a given location within a cloud follow different trajectories through a cloud. Variability of the supersaturation along those trajectories results in broadening of the droplet distribution. The supersaturation variability comes from relatively large turbulent eddies (scales from meters to hundreds of meters), often resulting from cloud-edge instabilities and entrainment. Cloud droplets "hop" those eddies and grow in response to local fluctuations of the supersaturation. This mechanism was suggested several decades ago by Cooper (1989), and it was investigated in subsequent studies (e.g., Lasher-Trapp et al. 2005; Cooper et al. 2013). Lasher-Trapp et al. (2005) combined a 3D Eulerian dynamic cloud model and a sophisticated Lagrangian trajectory model to study the eddy-hopping mechanism. They were able to represent key features of observed cumulus droplet spectra: large width, presence of small droplet well above the cloud base, and multimodal shape of the droplet spectrum. In a more idealized study, Sidin et al. (2009) investigated growth of Lagrangian droplets embedded within a synthetic 2D turbulence flow field and documented significant droplet spectra broadening as well.

The eddy-hopping mechanism can be conveniently investigated applying a Lagrangian cloud model. Such a model merges representation of the condensed water applying a set of Lagrangian cloud droplets and drizzle/rain drops [superdroplets using the terminology introduced by Shima et al. (2009)] with the Eulerian approach for the fluid flow and transport of water vapor and thermal energy. However, the model spatial resolution has to be high enough to resolve at least large turbulent eddies [as in the large-eddy simulation (LES)] and needs to include appropriate subgrid-scale (SGS) representation of unresolved turbulent eddies that affect superdroplet motion and growth/evaporation. Unfortunately, applications of Lagrangian cloud models (e.g., Shima et al. 2009; Andrejczuk et al. 2010; Riechelmann et al. 2012; Arabas et al. 2015) so far exclude the latter. This paper fills this gap and presents a relatively simple method to include impact of SGS processes on superdroplet growth. We apply the new SGS scheme to arguably the simplest system, a rising adiabatic parcel model, and document a significant widening of the cloud droplet spectrum in the turbulent adiabatic parcel.

The paper is organized as follows. The next section presents the adiabatic parcel model. Section 3 extends the adiabatic model to include turbulent velocity fluctuations that are the key in the eddy hoping mechanism and compares results that include the impact of turbulence to the results without turbulence. Section 4 concludes the paper with a brief discussion of model results.

2. Adiabatic parcel model

Equations for the adiabatic parcel model follow Grabowski and Wang (2009) and Grabowski et al. (2011), GW09, and GAW11, respectively. The temperature T and water vapor mixing ratio q_v for the parcel are functions of time only and their evolutions are given by

$$c_p \frac{dT}{dt} = -gw + L_v C \quad \text{and} \tag{1}$$

$$\frac{dq_v}{dt} = -C, \tag{2}$$

where w is the parcel vertical velocity, $g = 9.81\,\mathrm{m\,s^{-2}}$ is the gravitational acceleration, $L_v = 2.5 \times 10^6\,\mathrm{J\,kg^{-1}}$ is the latent heat of vaporization, $c_p = 1005\,\mathrm{J\,kg^{-1}\,K^{-1}}$ is the specific heat of air at constant pressure, and C is the condensation rate. The pressure p within the parcel is assumed to decrease with height as in the hydrostatically balanced environment:

$$\frac{dp}{dt} = -\rho_0 wg, \tag{3}$$

where ρ_0 is the air density. As in GW09, we assume $\rho_0 = 1\,\mathrm{kg\,m^{-3}}$ that corresponds to the shallow convection approximation. Such an approach is justified by relatively small vertical parcel displacements considered in this study, up to 1 km. The initial conditions for the parcel are as in GW09; that is, $T(t = 0) = 288.16\,\mathrm{K}$, $p(t = 0) = 900\,\mathrm{hPa}$, and relative humidity (RH) of 99%. The parcel vertical velocity is selected as $w = 1\,\mathrm{m\,s^{-1}}$.

Once RH inside the parcel passes 100%, activation of cloud droplets commences. We apply the Twomey activation (Twomey 1959) with cloud condensation nuclei (CCN) characteristics that include the number of activated CCN for a given supersaturation and the activation radius. We assume idealized CCN distribution as a sum of two lognormal distributions with concentrations, mean radii, and geometric standard deviations (unitless) as 60 and $40\,\mathrm{cm^{-3}}$, 20 and 75 nm, and 1.4 and 1.6, respectively. Integration of the lognormal distribution provides the Twomey relationship (i.e., the concentration of activated CCN N versus the supersaturation S; the N–S relationship) that is tabulated in the current study and used as input to the parcel model.

Figure 1 shows the Twomey N–S relationship resulting from the assumed CCN and explains how activated droplets are introduced to the parcel. First, the maximum supersaturation $S_{\max}$ is selected. By requirement, $S_{\max}$ has to exceed the maximum supersaturation

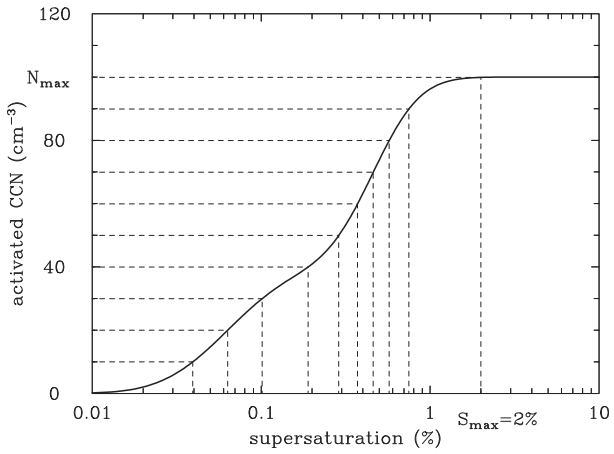

FIG. 1. Thick line represents the Twomey N–S relationship used in the current study. Dashed thin lines demonstrate how superdroplets are introduced in the activation scheme. See text for details.

experienced by the parcel. In the current study, $S_{max} = 2\%$ is used. The corresponding droplet concentration N_{max} is divided by the number of droplet classes to be used in the simulations. The example in Fig. 1 assumes 10 classes whereas model simulations apply 20 000 classes (most of results do not change once the number exceeds several hundreds). Note that these classes can be considered as superdroplets (Shima et al. 2009). As the supersaturation builds up near the cloud base, individual superdroplets are introduced when the predicted supersaturation exceeds the supersaturation corresponding to the activation supersaturation of already present superdroplets. Such an approach ensures that the multiplicity parameter (i.e., the number mixing ratio of droplets that a single superdroplet represents) is constant for all superdroplets. Once activated, the initial radius corresponding to the activation radius is assigned for each superdroplet. The latter is approximated as $8 \times 10^{-10}/S_{act}$, where S_{act} is the activation supersaturation; see Eq. (6) and Fig. 2 in GAW11. In addition to the droplet radius, the model keeps track of the superdroplet number mixing ratio (i.e., the number of droplets per unit mass of dry air) that corresponds to the multiplicity parameter (or attribute) of Shima et al. (2009). Superdroplet position is irrelevant and it is excluded from the list of superdroplet attributes in the current study. We note in passing that GAW11 includes a detailed comparison between comprehensive activation scheme (i.e., keeping track of the wet CCN radius prior to activation) and the much more efficient Twomey approach. The two methods give similar results except near the cloud base where deliquesence and eventual CCN activation takes place (see Figs. 4–7 in GAW11).

The diffusional growth rate of a cloud droplet is given by a simplified formula neglecting the curvature and solute effects but including the kinetic effects (see GAW11 and references therein):

$$\frac{dr}{dt} = \frac{1}{r + r_0} AS, \tag{4}$$

where r is the droplet radius, $S = q_v/q_{vs} - 1$ is the supersaturation (q_{vs} is the water vapor mixing ratio at saturation), $A = 0.9152 \times 10^{-10}\,\mathrm{m^2\,s^{-1}}$, and the kinetic effects are included through the parameter r_0 taken as $1.86\,\mu$m (e.g., Clark 1974; Kogan 1991). The condensation rate is derived from the rate of change of the droplet population mass:

$$C = \frac{d}{dt} \sum_i \frac{4}{3} \pi r_i^3 N_i \frac{\rho_w}{\rho_0}, \tag{5}$$

where N_i is the number mixing ratio for the superdroplet of radius r_i and $\rho_w = 10^3\,\mathrm{kg\,m^{-3}}$ is the water density.

Parcel model equations are integrated applying a simple Euler forward scheme and a 0.2-s time step. Figure 2 shows selected results from the adiabatic parcel model simulation. The bottom four panels document evolution of key parameters, and the top panels depict the spectrum at the end of the simulation (i.e., for $t = 1000$ s) using either linear or logarithmic scale. The spectrum is calculated by grouping all superdroplets into a regular radius grid with a 0.2-μm bin size. Saturation within the parcel is reached in a few tens of meters and droplet activation begins. Activation continues until the supersaturation reaches its peak of about 0.9% within subsequent few tens of meters. As the parcel continues to rise, the droplet mean radius and the liquid water mixing ratio increase, and the standard deviation of the droplet distribution (referred to as the spectral width σ) decreases. At the end of the simulation, the width is relatively small, around $0.3\,\mu$m, in agreement with the adiabatic growth of a droplet population (e.g., Brenguier and Chaumat 2001). A peculiar feature of the size distribution, the peak in the bin corresponding to the largest droplet size, is because of a particular detail of the Twomey activation scheme applied. This is because no droplet activation is allowed for supersaturations smaller than the lowest bin in the tabulated N–S relationship, 0.01% in the current application. Thus, once the 0.01% threshold is passed, the first class of superdroplets receives all droplets corresponding to $S < 0.01\%$. That number is larger than in subsequent activation bins because of the large number of superdroplet bins (20 000) used in the simulations. Applying linear interpolation between $S = 0\%$ and $S = 0.01\%$ leads to unrealistically large activation radii (say, larger than several micrometers) that in reality require long

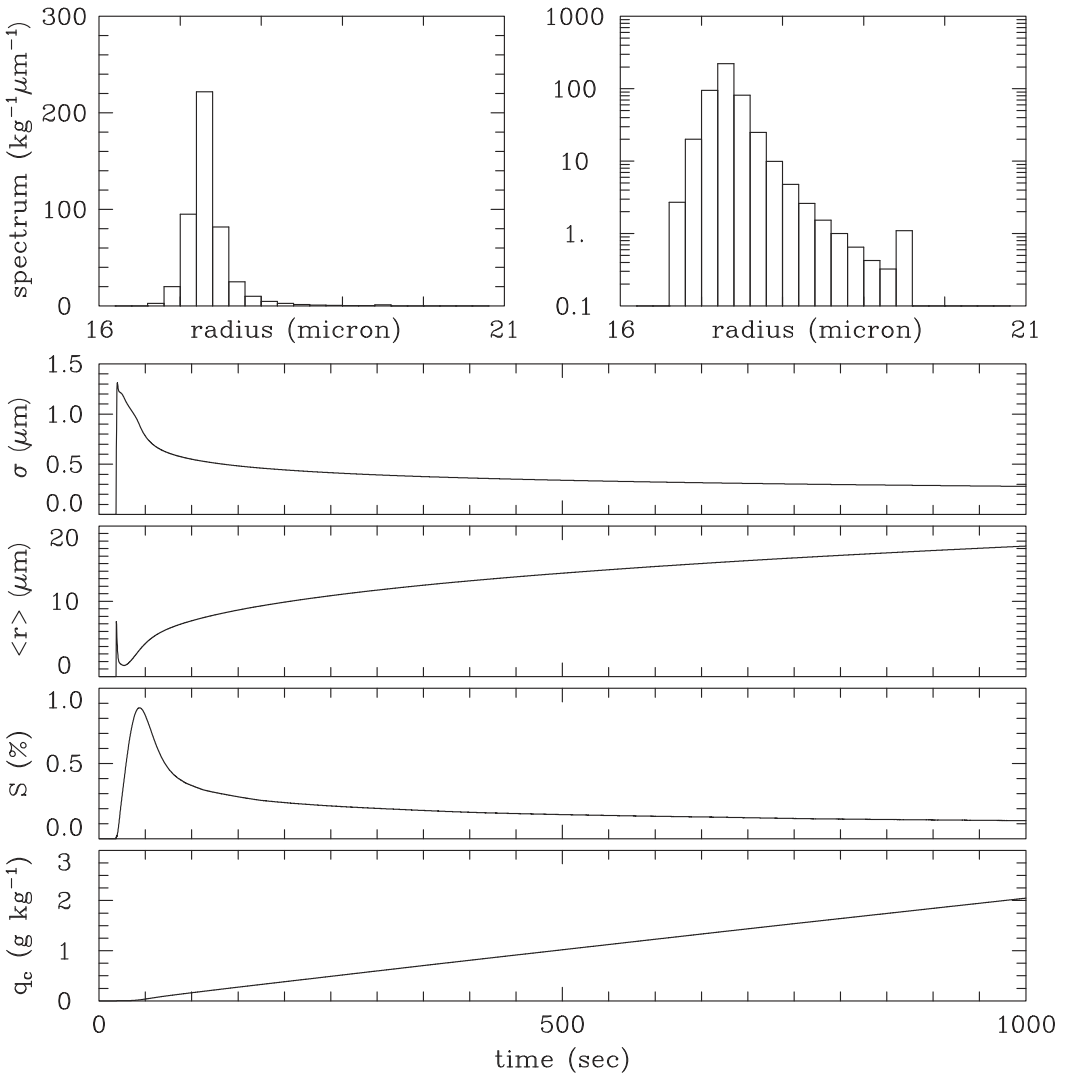

FIG. 2. (bottom) Evolutions of (from the lowest to the highest) total cloud water q_c, supersaturation S (with only positive values shown), mean droplet radius $\langle r \rangle$, and spectral width σ. (top) Droplet spectra at $t = 1000$ s applying (left) a linear and (right) a logarithmic scale of the vertical axis.

time (often hundreds of seconds) before they reach the activation radius [e.g., Barahona et al. (2010) and references therein]. This is a general problem when the Twomey activation is applied to giant and ultragiant CCN, but this aspect has no implications for the comparison documented here.

3. Turbulent adiabatic parcel model

a. Formulation

The turbulent adiabatic parcel model assumes that the parcel is filled with isotropic homogeneous turbulence. Eddy hopping of each superdroplet is represented by supersaturation fluctuations that the superdroplet experiences as the parcel rises with the prescribed updraft. Thus, droplets in the proposed scheme do not physically hop turbulent eddies; only the effect of hopping is represented in the droplet growth equation.

There are two parameters that determine the turbulence inside the parcel: 1) the dissipation rate ε of the turbulent kinetic energy (TKE) that describes intensity of the turbulence and 2) the extent L of the adiabatic parcel. The two parameters determine TKE E and the integral time scale τ of the turbulence inside the parcel. We assume that for the isotropic homogeneous turbulence

$$E = \left(\frac{L\varepsilon}{C_E}\right)^{2/3} \tag{6}$$

TABLE 1. TKE ($m^2 s^{-2}$; top number) and integral time scale τ (s; bottom number) for various length scales L (size of the parcel) and TKE dissipation rates ε.

	ε ($cm^2 s^{-3}$)			
L (m)	1	10	100	1000
1	2.4×10^{-3} 14	1.1×10^{-2} 6.3	5.2×10^{-2} 2.9	0.24 1.4
10	1.1×10^{-2} 63	5.2×10^{-2} 29	0.24 14	1.1 6.3
100	5.2×10^{-2} 291	0.24 135	1.1 63	5.2 29
1000	0.24 1.35×10^{3}	1.1 627	5.2 291	24 135

and

$$\tau = \frac{L}{(2\pi)^{1/3}} \left(\frac{C_\tau}{E}\right)^{1/2}, \tag{7}$$

with $C_E = 0.845$ (Schumann 1991) and $C_\tau = 1.5$ as in Lasher-Trapp et al. (2005).

Table 1 illustrates variability of E and τ as a function of ε (between 1 and 1000 $cm^2 s^{-3}$) and L (between 1 and 1000 m). For a given dissipation rate, TKE increases with the increase of the length scale L. This is because TKE comes predominantly from subgrid-scale motions of scales not much smaller than the scale L (i.e., the $-5/3$ scaling). By the same token, the integral time scale increases with the increase of the length scale L for a given dissipation rate because it can be thought as a time scale dominated by the largest SGS turbulent eddies. TKE increases and the integral time scale decreases with the increase of the dissipation rate for a given spatial scale L because SGS eddies become more vigorous.

In the specific problem considered here, TKE determines velocity fluctuations and thus the supersaturation perturbations that each droplet experiences as a result of turbulence. The local supersaturation perturbation S_i' for the superdroplet i (from the mean supersaturation S predicted by the adiabatic parcel equations) is used as additional attribute of each superdroplet. Its evolution is given by [see Squires (1952), Politovich and Cooper (1988), and references therein]

$$\frac{dS_i'}{dt} = a_1 w' - \frac{S_i'}{\tau_{\text{relax}}}, \tag{8}$$

where w' is the vertical velocity perturbation experienced by the superdroplet, $a_1 = 3 \times 10^{-4}\ m^{-1}$, and τ_{relax} is the phase relaxation time scale of the droplet population. The latter is given as [see Squires (1952), Cooper (1989), Grabowski and Wang (2013), and references therein]

$$\tau_{\text{relax}} = \left(a_2 \sum_i r_i N_i\right)^{-1}, \tag{9}$$

where $a_2 = 2.8 \times 10^{-4}\ m^2 s^{-1}$.

It is important to stress that τ_{relax} is not given by the local environment of a superdroplet [as, for instance, in DNS simulations of Vaillancourt et al. (2002) and others following the approach advocated by Srivastava (1989)] but by the entire superdroplet population.[1] This is because each superdroplet represents multiplicity of droplets in the well-mixed parcel. In other words, local droplet size distribution is exactly the same as the distribution averaged over the entire parcel volume. For the same reason, the impact documented in the current study represents a lower bound of the eddy hoping impact within the adiabatic turbulent parcel. Allowing spatial variability of τ_{relax} will lead to an even larger effect than the one documented here.

We assume the vertical velocity perturbation w' is a random stationary process known as the Ornstein–Uhlenbeck process (e.g., Pope 1994) and it serves a crude representation of velocity perturbations due to range of SGS eddies of the homogeneous isotropic turbulence. The perturbation is assumed to evolve according to the update equation (e.g., Lemons 2002):

$$w'(t + \delta t) = w'(t) e^{-\delta t/\tau} + \sqrt{1 - e^{-2\delta t/\tau}}\, \sigma_{w'} \psi, \tag{10}$$

where δt is the model time step, $\sigma_{w'}^2$ is the vertical velocity variance obtained from TKE as

$$\sigma_{w'}^2 = \frac{2}{3} E, \tag{11}$$

τ is the integral time scale of turbulence defined in Eq. (7), and ψ is a Gaussian random number with zero mean and unit variance drawn every time step. Then w' is used to evolve the supersaturation perturbation S' [see (8)] experienced by the superdroplet and S' is added to the mean supersaturation S to calculate a given superdroplet growth [see (4)].

In summary, the eddy dissipation rate ε and the scale L of the adiabatic parcel determine the vertical velocity perturbations that affect the local supersaturation perturbations S' and allow each superdroplet growing in a stochastic manner. It needs to be stressed that such an approach is a relatively simple model of the supersaturation fluctuations experienced by cloud droplets during eddy hopping. For instance, one can envision a more sophisticated model of supersaturation

[1] This implies that our results cannot be directly compared to the DNS simulation results.

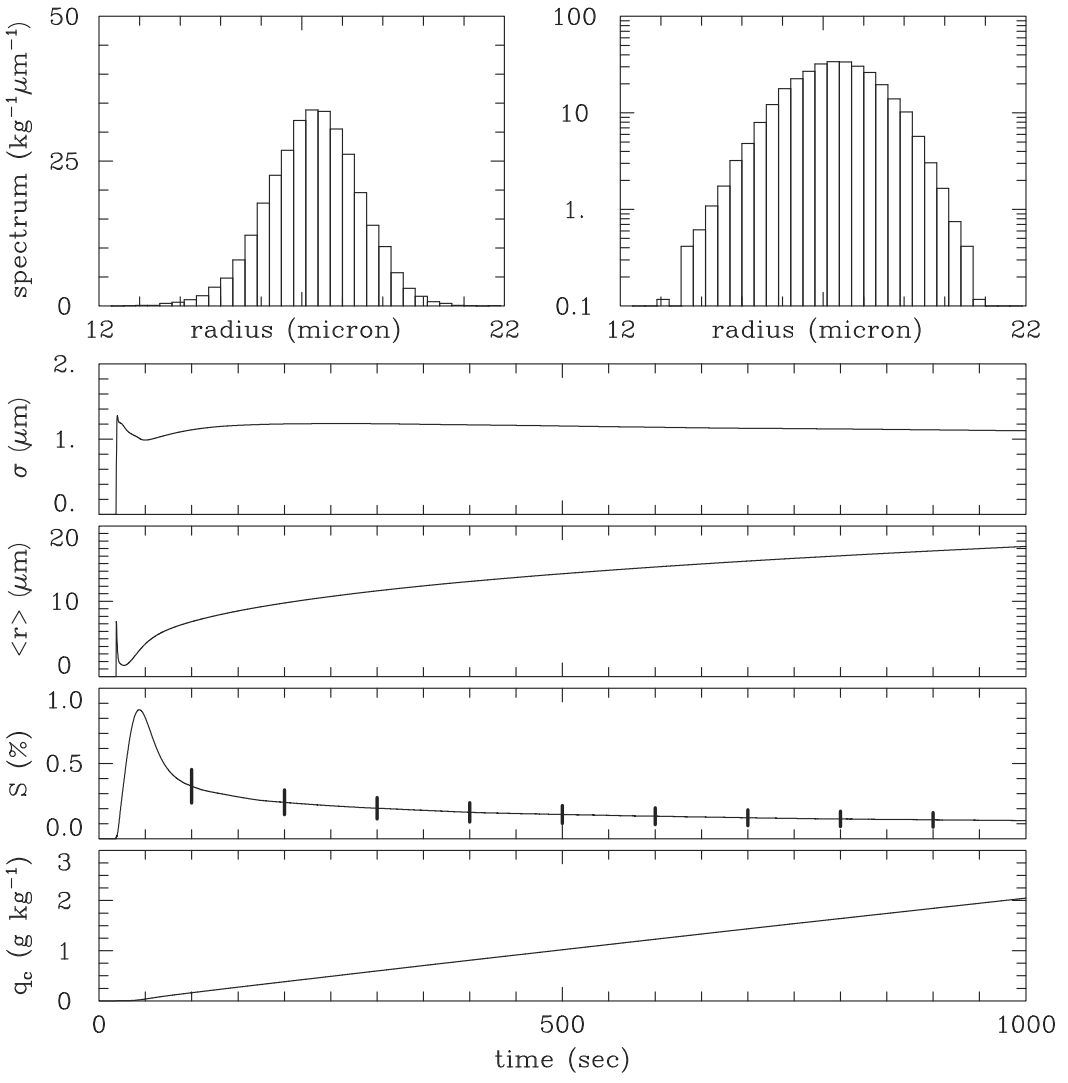

FIG. 3. As in Fig. 2, but for the turbulent adiabatic parcel with $L = 50$ m and $\varepsilon = 50\,\mathrm{cm^2\,s^{-3}}$. The thick vertical lines at 100-s intervals in the plot of S represent twice the standard deviation of the S distribution among all superdroplets. Please note a larger scale on the vertical axis in the plot of σ and a larger range of radii for the top panels when compared to Fig. 2.

fluctuations—for instance, including effects of non-Gaussian velocity distribution due to flow intermittency or other departures from isotropy and local homogeneity. Such extensions of the SGS scheme proposed here should be investigated in the future.

b. Results

Figure 3 shows example of results for the turbulent adiabatic parcel for $L = 50$ m [i.e., the grid length used in Lasher-Trapp et al. (2005) simulations] and $\varepsilon = 50\,\mathrm{cm^2\,s^{-3}}$. This arguably corresponds to an adiabatic core of a cumulus cloud with typical for cumulus levels of turbulence (e.g., Jonas 1996; Pruppacher and Klett 1997). The most significance difference between Figs. 2 and 3 is an increased spectral width. For the adiabatic parcel (Fig. 2), the width decreases after the activation is completed, and it is around 0.3 μm at the end of the simulation. For the turbulent parcel, the width stays around 1 μm throughout the most of the simulation. The supersaturation fluctuations are significant, with the standard deviation among the superdroplets comparable to the parcel mean supersaturation.

Figure 4 shows the mean radius and spectral width at the end of simulations (i.e., at $t = 1000$ s) as a function of the scale L for different eddy dissipation rates ε. The impact of turbulence is significant, and it increases with the increase of the parcel extent and with the increase of the eddy dissipation rate. For spatial scales smaller than

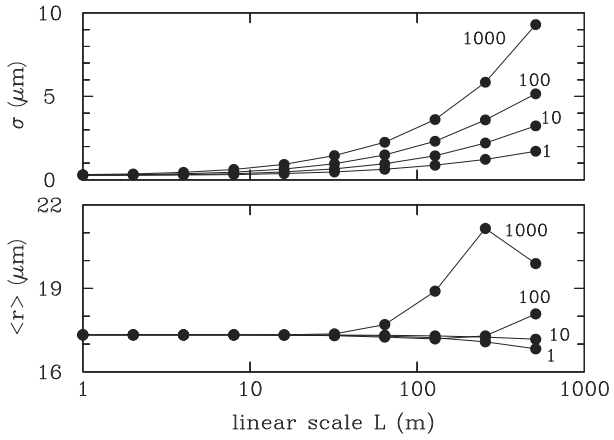

FIG. 4. Mean radius and spectral width at $t = 1000$ s as a function of the scale L for different eddy dissipation rates ε ($\mathrm{cm^2\,s^{-3}}$). The simulation data (dots) are connected by lines to guide the eye.

10 m, the impact of the turbulence is small. This agrees with numerous DNS studies that show minimal spectral broadening in simulations that are limited to small computations domains, typically a fraction of $1\,\mathrm{m}^3$ (e.g., Vaillancourt et al. 2002; Lanotte et al. 2009). One has to keep in mind, however, that our simulations represent the lower bound of the impact as mentioned before and cannot be directly compared with DNS. Only when the scale is larger than a few tens of meters, turbulence starts to show some impact, and the impact is especially significant for large TKE dissipation rates. For scales of a few hundred meters, the impact is large, with the spectral width increasing up to several micrometers, an order of magnitude larger than in the adiabatic parcel without turbulence.

The mean radius is also affected when L is larger than several tens of meters. For large-ε, large-L cases, the explanation has to do with complete evaporation of some droplets above the cloud base because of the magnitude and persistence of the supersaturation perturbations. In such cases, the scheme simulates the so-called super-adiabatic growth of the droplet population: by removing some droplets, the mean droplet concentration decreases and the remaining population grows beyond the mean adiabatic size—hence the name. The superadiabatic growth is typically argued to result from reduction of the droplet concentration due to entrainment/mixing, but apparently it can also operate as a result of large and energetic turbulent eddies in the rising adiabatic parcel framework. The small decrease of the mean radius for weak and moderate ε and large L comes from additional activation of cloud droplets due to positive supersaturation fluctuations. This leads to a slight increase of the mean droplet concentration and thus small decrease of the radius after a 1-km parcel raise.

4. Discussion and conclusions

Idealized adiabatic parcel model simulations clearly show that including subgrid-scale vertical velocity fluctuations experienced by superdroplets is important for the broadening of the droplet spectra. This especially applies to large-eddy simulations with model grid length of a few tens of meters. For instance, applying the length scale L of 50 m, the same as the model grid length used in the LES in Lasher-Trapp et al. (2005), and the CCN characteristics considered here increases the spectral width from 0.3 μm for the adiabatic parcel without turbulence at the end of the simulation (1-km vertical displacement) to over 0.8 and about 1.3 μm for eddy dissipations of 10 and $100\,\mathrm{cm^2\,s^{-3}}$, respectively. Such broadening can significantly accelerate formation of drizzle drops through collision–coalescence (Cooper et al. 2013). As comparison of Figs. 2 and 3 shows, turbulence can virtually suppress narrowing of the droplet spectrum due to the parabolic (i.e., $dr^2/dt \approx$ const) droplet growth.

The pilot investigation presented here can be easily extended into different aerosol conditions (e.g., using CCN characteristics of a polluted environment), different thermodynamic conditions (pressure and temperature), as well as different mean updraft velocities. Simulations with the updraft of $5\,\mathrm{m\,s^{-1}}$ instead of $1\,\mathrm{m\,s^{-1}}$ discussed in the previous section and the same vertical displacement (1 km) show smaller but still significant impacts of eddy hopping. For instance, the spectral width increases from 0.24 μm for the adiabatic parcel without turbulence to 0.47 μm for the turbulent parcel with L of 50 m and eddy dissipations of $50\,\mathrm{cm^2\,s^{-3}}$. Reduction of the impact for the same vertical displacement is arguably consistent with a reduced time available for hopping turbulent eddies and developing significant spread of droplet growth histories.

Finally, the supersaturation fluctuation scheme developed here can be easily implemented in the LES Lagrangian cloud model in addition to the SGS velocity fluctuations that affect motion of Lagrangian superdroplets. TKE is typically predicted by the SGS scheme (or can be diagnosed if a Smagorinsky SGS scheme is used) and the appropriate scale L should be taken as the LES filter scale [e.g., $(\Delta x \Delta y \Delta z)^{1/3}$ as commonly used]. Results presented here suggest that such an extension can significantly add to the impact discussed in Lasher-Trapp et al. (2005) and in Cooper et al. (2013) where eddy hopping associated with interfacial instabilities and entrainment/mixing was the focus. We expect that

representation of entrainment/mixing (excluded in the adiabatic parcel model) can also be incorporated into our methodology by developing a more comprehensive SGS supersaturation equation—for instance, as in the study of Paoli and Shariff (2009). We are exploring such possibilities in ongoing research.

Acknowledgments. This work was partially supported by the Polish National Science Center (NCN) ''POLONEZ 1'' Grant 2015/19/P/ST10/02596 and by the U.S. DOE ASR Grant DE-SC0016476. The POLONEZ 1 grant has received funding from the European Union's Horizon 2020 Research and Innovation Program under the Marie Sklodowska-Curie Grant Agreement 665778.

REFERENCES

Andrejczuk, M., W. W. Grabowski, J. Reisner, and A. Gadian, 2010: Cloud-aerosol interactions for boundary layer stratocumulus in the Lagrangian cloud model. *J. Geophys. Res.*, **115**, D22214, doi:10.1029/2010JD014248.

Arabas, S., A. Jaruga, H. Pawlowska, and W. W. Grabowski, 2015: libcloudph++ 1.0: A single-moment bulk, double-moment bulk, and particle-based warm-rain microphysics library in C++. *Geosci. Model Dev.*, **8**, 1677–1707, doi:10.5194/gmd-8-1677-2015.

Barahona, D., R. E. L. West, P. Stier, S. Romakkaniemi, H. Kokkola, and A. Nenes, 2010: Comprehensively accounting for the effect of giant CCN in cloud activation parameterizations. *Atmos. Chem. Phys.*, **10**, 2467–2473, doi:10.5194/acp-10-2467-2010.

Brenguier, J.-L., and L. Chaumat, 2001: Droplet spectra broadening in cumulus clouds. Part I: Broadening in adiabatic cores. *J. Atmos. Sci.*, **58**, 628–641, doi:10.1175/1520-0469(2001)058<0628:DSBICC>2.0.CO;2.

Clark, T. L., 1974: On modelling nucleation and condensation theory in Eulerian spatial domain. *J. Atmos. Sci.*, **31**, 2099–2117, doi:10.1175/1520-0469(1974)031<2099:OMNACT>2.0.CO;2.

Cooper, W. A., 1989: Effects of variable droplet growth histories on droplet size distributions. Part I: Theory. *J. Atmos. Sci.*, **46**, 1301–1311, doi:10.1175/1520-0469(1989)046<1301:EOVDGH>2.0.CO;2.

——, S. G. Lasher-Trapp, and A. M. Blyth, 2013: The influence of entrainment and mixing on the initial formation of rain in a warm cumulus cloud. *J. Atmos. Sci.*, **70**, 1727–1743, doi:10.1175/JAS-D-12-0128.1.

Grabowski, W. W., and L.-P. Wang, 2009: Diffusional and accretional growth of water drops in a rising adiabatic parcel: Effects of the turbulent collision kernel. *Atmos. Chem. Phys.*, **9**, 2335–2353, doi:10.5194/acp-9-2335-2009.

——, and ——, 2013: Growth of cloud droplets in a turbulent environment. *Annu. Rev. Fluid Mech.*, **45**, 293–324, doi:10.1146/annurev-fluid-011212-140750.

——, M. Andrejczuk, and L.-P. Wang, 2011: Droplet growth in a bin warm-rain scheme with Twomey CCN activation. *Atmos. Res.*, **99**, 290–301, doi:10.1016/j.atmosres.2010.10.020.

Jensen, J., P. Austin, M. Baker, and A. Blyth, 1985: Turbulent mixing, spectral evolution and dynamics in a warm cumulus cloud. *J. Atmos. Sci.*, **42**, 173–192, doi:10.1175/1520-0469(1985)042<0173:TMSEAD>2.0.CO;2.

Jonas, P., 1996: Turbulence and cloud microphysics. *Atmos. Res.*, **40**, 283–306, doi:10.1016/0169-8095(95)00035-6.

Kogan, Y. L., 1991: The simulation of a convective cloud in a 3-D model with explicit microphysics. Part I: Model description and sensitivity experiments. *J. Atmos. Sci.*, **48**, 1160–1189, doi:10.1175/1520-0469(1991)048<1160:TSOACC>2.0.CO;2.

Lanotte, A. S., A. Seminara, and F. Toschi, 2009: Cloud droplet growth by condensation in homogeneous isotropic turbulence. *J. Atmos. Sci.*, **66**, 1685–1697, doi:10.1175/2008JAS2864.1.

Lasher-Trapp, S. G., W. A. Cooper, and A. M. Blyth, 2005: Broadening of droplet size distributions from entrainment and mixing in a cumulus cloud. *Quart. J. Roy. Meteor. Soc.*, **131**, 195–220, doi:10.1256/qj.03.199.

Lemons, D. S., 2002: *An Introduction to Stochastic Processes in Physics.* Johns Hopkins University Press, 128 pp.

Paoli, R., and K. Shariff, 2009: Turbulent condensation of droplets: Direct simulation and a stochastic model. *J. Atmos. Sci.*, **66**, 723–740, doi:10.1175/2008JAS2734.1.

Pawlowska, H., W. W. Grabowski, and J.-L. Brenguier, 2006: Observations of the width of cloud droplet spectra in stratocumulus. *Geophys. Res. Lett.*, **33**, L19810, doi:10.1029/2006GL026841.

Politovich, M. K., and W. A. Cooper, 1988: Variability of the supersaturation in cumulus clouds. *J. Atmos. Sci.*, **45**, 1651–1664, doi:10.1175/1520-0469(1988)045<1651:VOTSIC>2.0.CO;2.

Pope, S. B., 1994: Lagrangian PDF methods for turbulent flows. *Annu. Rev. Fluid Mech.*, **26**, 23–63, doi:10.1146/annurev.fl.26.010194.000323.

Prabha, T. V., and Coauthors, 2012: Spectral width of premonsoon and monsoon clouds over Indo-Gangetic valley. *J. Geophys. Res.*, **117**, D20205, doi:10.1029/2011JD016837.

Pruppacher, H. R., and J. D. Klett, 1997: *Microphysics of Clouds and Precipitation.* Atmospheric and Oceanographic Sciences Library, Vol. 18, Springer, 954 pp.

Riechelmann, T., Y. Noh, and S. Raasch, 2012: A new method for large-eddy simulations of clouds with Lagrangian droplets including the effects of turbulent collision. *New J. Phys.*, **14**, 065008, doi:10.1088/1367-2630/14/6/065008.

Schumann, U., 1991: Subgrid length-scales for large-eddy simulation of stratified turbulence. *Theor. Comput. Fluid Dyn.*, **2**, 279–290, doi:10.1007/BF00271468.

Shima, S., K. Kusano, A. Kawano, T. Sugiyama, and S. Kawahara, 2009: The super-droplet method for the numerical simulation of clouds and precipitation: A particle-based and probabilistic microphysics model coupled with a non-hydrostatic model. *Quart. J. Roy. Meteor. Soc.*, **135**, 1307–1320, doi:10.1002/qj.441.

Sidin, R. S. R., R. H. A. IJzermans, and M. W. Reeks, 2009: A Lagrangian approach to droplet condensation in atmospheric clouds. *Phys. Fluids*, **21**, 106603, doi:10.1063/1.3244646.

Squires, P., 1952: The growth of cloud drops by condensation. I. General characteristics. *Aust. J. Sci. Res.*, **5A**, 66–86.

Srivastava, R. C., 1989: Growth of cloud drops by condensation: A criticism of currently accepted theory and a new approach. *J. Atmos. Sci.*, **46**, 869–887, doi:10.1175/1520-0469(1989)046<0869:GOCDBC>2.0.CO;2.

Su, C.-W., S. K. Krueger, P. A. McMurtry, and P. H. Austin, 1998: Linear eddy modeling of droplet spectral evolution during entrainment and mixing in cumulus clouds. *Atmos. Res.*, **47–48**, 41–58, doi:10.1016/S0169-8095(98)00039-8.

Twomey, S., 1959: The nuclei of natural cloud formation. Part II: The supersaturation in natural clouds and the variation of cloud

droplet concentration. *Pure Appl. Geophys.*, **43**, 243–249, doi:10.1007/BF01993560.

Vaillancourt, P. A., M. K. Yau, P. Bartello, and W. W. Grabowski, 2002: Microscopic approach to cloud droplet growth by condensation. Part II: Turbulence, clustering, and condensational growth. *J. Atmos. Sci.*, **59**, 3421–3435, doi:10.1175/1520-0469(2002)059<3421:MATCDG>2.0.CO;2.

Warner, J., 1969a: The microstructure of cumulus cloud. Part I: General features of the droplet spectrum. *J. Atmos. Sci.*, **26**, 1049–1059, doi:10.1175/1520-0469(1969)026<1049:TMOCCP>2.0.CO;2.

——, 1969b: The microstructure of cumulus cloud. Part II: The effect on droplet size distribution of the cloud nucleus spectrum and updraft velocity. *J. Atmos. Sci.*, **26**, 1272–1282, doi:10.1175/1520-0469(1969)026<1272:TMOCCP>2.0.CO;2.

——, 1970: The microstructure of cumulus cloud. Part III: The nature of the updraft. *J. Atmos. Sci.*, **27**, 682–688, doi:10.1175/1520-0469(1970)027<0682:TMOCCP>2.0.CO;2.

——, 1973a: The microstructure of cumulus cloud. Part IV: The effect on the droplet spectrum of mixing between cloud and environment. *J. Atmos. Sci.*, **30**, 256–261, doi:10.1175/1520-0469(1973)030<0256:TMOCCP>2.0.CO;2.

——, 1973b: The microstructure of cumulus cloud. Part V: Changes in droplet size distribution with cloud age. *J. Atmos. Sci.*, **30**, 1724–1726, doi:10.1175/1520-0469(1973)030<1724:TMOCCP>2.0.CO;2.